Pattern transfer, self-organized surface nanostructuring, and nanodrilling of sapphire using nanosecond laser irradiation

P. Lorenz*, J. Zajadazc, M. Ehrhardt, L. Bayer, K. Zimmer

Leibniz-Institut für Oberflächenmodifizierung e. V., Permoserstr. 15, 04318 Leipzig, Germany

ABSTRACT

Nanostructures have a widespread field of applications. The structuring of sapphire assisted by a nanosecond laser-induced self-organized molten molybdenum layer deformation process was studied. At low laser fluence the irradiation of a thin metal layer on dielectric surface results in a melting and nanostructuring of the metal layer and partially of the dielectric surface. Furthermore, a subsequent high laser fluence treatment of the metal nanostructures results in different features: (i) pattern transfer, (ii) self-organized surface nanostructuring, and (iii) nanodrilling. (i) Pattern transfer: The irradiation of the pre-structured metal layer with high laser fluences allows the transfer of the lateral geometry of the metal nanostructures into the dielectric surface. (ii) Self-organized surface nanostructuring: The multi-pulse irradiation of the metal layer/dielectric system with moderate laser fluences results in a self-organized nanostructuring of the dielectric surface. (iii) Nanodrilling: The multi-pulse low laser fluence irradiation of the metal layer results in the formation of metal droplets and a further high fluence irradiation of the laser-generated metal droplets results in a stepwise evaporation of the metal and in a partial evaporation of the dielectric and, finally, in the formation of cone-like holes. The resultant structures were investigated by scanning electron microscopy (SEM).

Keywords: nanosecond laser, nanostructuring, sapphire, pattern transfer, nanodrilling

1. INTRODUCTION

The fast and large-area mirco- and nanostructuring of dielectric surfaces especially using self-organized processes is a challenge for laser methods. Different laser-induced self-organization effects are known like the fs laser-induced ripple structure process[1–4], the fs laser metal nanostructuring process[5–7], as well as the ns laser nanostructuring process of metal layers[8-10]. Further, the direct ablation process with short[11, 12] and ultrashort laser pulses[13–16] allows the well-defined structuring of different materials. Besides the direct ablation process also indirect processes like: Laser-induced front side etching (LIFE), LIFE using self-regenerating adsorbed layer (SAL-LIFE), Laser-induced back side dry etching (LIBDE), Laser-induced back side wet etching (LIBWE), and laser etching at a surface-absorbed layer (LESAL)[17–20] allow the fabrication of vertical nm-precision and lateral sub-µm-precision structures in dielectrics with a very low surface roughness. The laser-induced front side etching using in situ pre-structured metal layers (IPSM-LIFE)[21] combined the concept of the ns laser nanostructuring of metal layers (droplet formation) with the LIFE process. The IPSM-LIFE process was studied on fused silica covered by chromium[21] and molybdenum[22]. The IPSM-LIFE process can separate in two steps. STEP 1: The low fluence ns laser irradiation of a thin metal layer result in a melting of the metal. The surface tension of the liquid metal result in a mass transport and finally to a formation of metal nanostructures like metal droplets[8-10, 21, 23]. The laser metal nanostructuring process exhibit different physical effects: photon - solid interaction[24-30], phase transition, and solid - liquid interaction[10, 31–36]. The laser –solid interaction including the phase transition can be physically described by a heat equation and the solid - liquid interaction can be described by a modified Navier-Stokes equation[22]. STEP 2: The high laser fluence irradiation of homogeneous and structured metal on dielectric surfaces results in an ablation process of the metal and in a modification of the dielectric surfaces like nanoholes [22, 28–30]. The structuring process as well as the resultant structures can be simulated by finite element methods using heat equation[22, 37].

*pierre.lorenz@iom-leipzig.de; phone ++49 (0)341 235 3291; www.iom-leipzig.de

Laser-based Micro- and Nanoprocessing X, edited by Udo Klotzbach, Kunihiko Washio, Craig B. Arnold,
Proc. of SPIE Vol. 9736, 97361K · © 2016 SPIE · CCC code: 0277-786X/16/$18 · doi: 10.1117/12.2212122

2. EXPERIMENTAL SET-UP

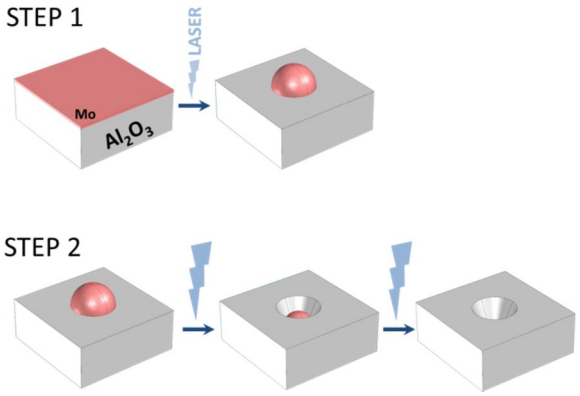

Figure 1. Schematic illustration of the laser-induced front side etching using in situ pre-structured metal layers (IPSM – LIFE) process at the example of the nanodrilling process. The IPSM-LIFE can be separated in two steps (Step 1: A low fluence irradiation of the metal covered dielectric substrate result in a nanostructuring of the metal layer.
Step 2: The high fluence irradiation result in a removal of the metal and to a structuring of the dielectric surface)

The IPSM-LIFE method was tested on sapphire covered with molybdenum. The molybdenum layer exhibit layer thickness of (20 ± 1) nm with a surface roughness of ~ 0.3 nm (rms) and a maximum peak-to-valley value of ~ 1 nm. Selective physical properties of the materials used are summarized in Tab. 1. The Mo/Al_2O_3 system was irradiated by a KrF excimer laser with a wavelength of λ = 248 nm, a pulse duration of Δt_p = 25 ns, and a repetition rate of f = 1–100 Hz. The utilized laser workstation comprises beam shaping and homogenizing optics, a x-y-z positioning stage, and a dielectric attenuator and provides an energy deviation in the mask plane of below 5% rms at a square laser spot with a spot size of A = 100 x 100 µm². The IPSM-LIFE can be split into two steps: STEP 1: low laser fluence irradiation and STEP 2: high laser fluence irradiation (see Fig. 1). At STEP 1: The Mo/Al_2O_3 system was irradiated with low laser fluences ($\Phi \leq 400$ mJ/cm²). The laser treatment results in the formation of randomly distributed metal structures like metal droplets. At STEP 2: The irradiation of the generated Mo structures with high laser fluences ($\Phi > 400$ mJ/cm²) result in a removal of the metal and to a structuring and modification of the sapphire surface.
The modification of the surface topography at STEP 1 and STEP 2 at different laser parameters (laser fluence Φ and number of laser pulses N) was analyzed by scanning electron microscopy (SEM). To exclude charging effects during the SEM measurements the samples was magnetron-sputtered with a ~10 nm thin gold.

Tab. 1 Selective physical properties of thematerials used [38–41].

	Al_2O_3	Mo
Density ρ [g/cm³] (T = 297.15 K)	3.98	10.28
Melting temperature T_m [K]	2303	2896
Boiling temperature T_{boi} [K]	3250	4912
Heat of fusion ΔH_m [kJ/mol]	14.15	37.48
Heat of vaporization ΔH_{boi} [kJ/mol]	1675.71	598
Molar heat capacity c [J/(mol*K)]	77.2 (290 K) 133.9 (1650 K)	24.06
R_{opt} (λ = 248 nm)	0.0885	0.6 – 0.68
thermal conductivity κ [W/(m*K)]	35	138
absorption coefficient [cm^{-1}]	~0	7.4
molare mass [g/mol]	101.96	95.94

3. RESULTS

i. Step 1 (low fluence irradiation)

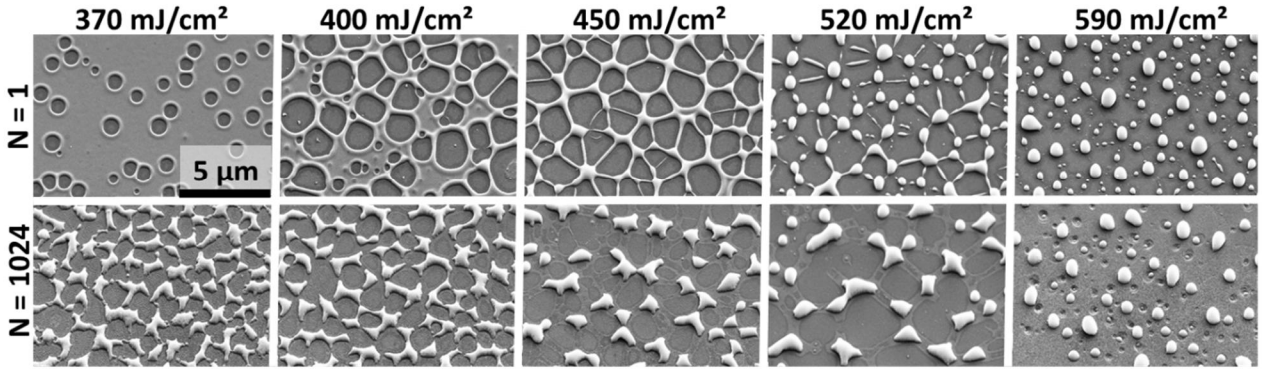

(a)

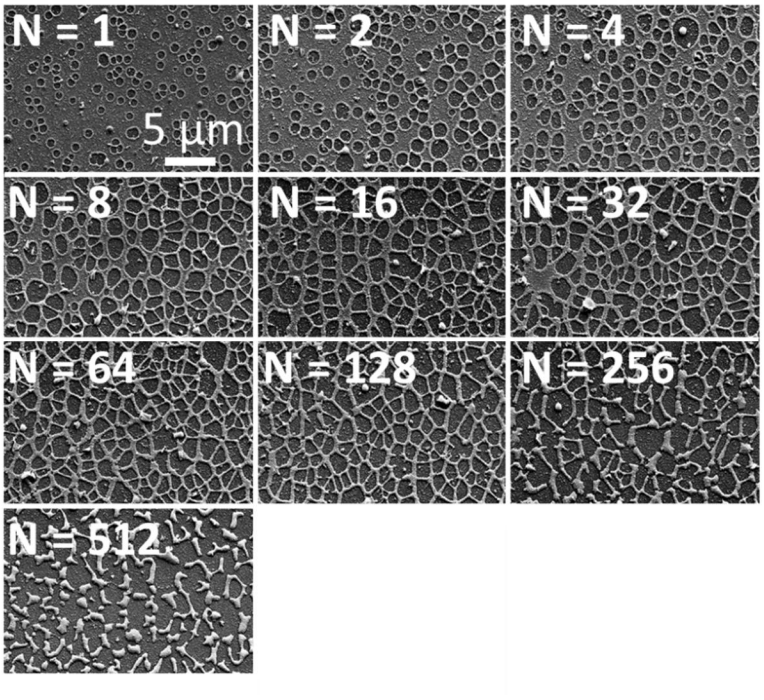

(b)

Figure 2. (a) SEM image of an irradiated 20 nm Mo layer on sapphire with different laser fluences at one and 1024 laser pulses. (b) SEM image of an irradiated 20 nm Mo on sapphire with 370 mJ/cm² at one and 1024 laser pulses

The low fluence irradiation of a 20 nm thick Mo layer on sapphire result in a pronounced modification of the surface morphology of the molybdenum layer where the resultant structures are dependent on the laser parameter: laser fluence and number of laser pulses (see Fig. 2).

The irradiation of the system results in a melting and transformation of the morphology of the Mo layer mainly induced by the surface tension of the liquid metal film[23]. The dewetting and droplet formation process start with the formation of hole structures (see e.g. Fig. 2 (a) N = 1, $\Phi \approx 370$ mJ/cm²). At $\Phi \approx 370$ mJ/cm² and N = 1 an average hole diameter of (580 ± 300) nm can be found. The size of the holes can be increased by further irradiation, see Fig. 2 (b). Further, the size of the holes can influence by the variation of the laser fluence, the hole size increased at increasing laser fluence. The increasing of the holes results in a coalescence of the molybdenum and results finally to

the formation of metal droplets (see e.g. Fig. 2 (a), N = 1, Φ ≈ 590 mJ/cm²) After the irradiation of the Mo/Al_2O_3 system with one laser pulse and 590 mJ/cm² metal droplet in the size from ~150 to ~800 nm can be detected
Similar effects were found at the irradiation of molybdenum. Furthermore, at adequate laser fluence and multi pulse irradiation the laser treatment result in the modification of the fused silica surface besides the droplet formation process (see Fig. 2 (a) Φ ≈ 590 mJ/cm², N = 1024). The SEM images presented that the multi pulse irradiation result in a circular structure into the fused silica surface where the distribution and size of the structures is mainly defined by the position and size of the formed metal droplets.

ii. Step 2 (high fluence irradiation)

(a) pattern transfer

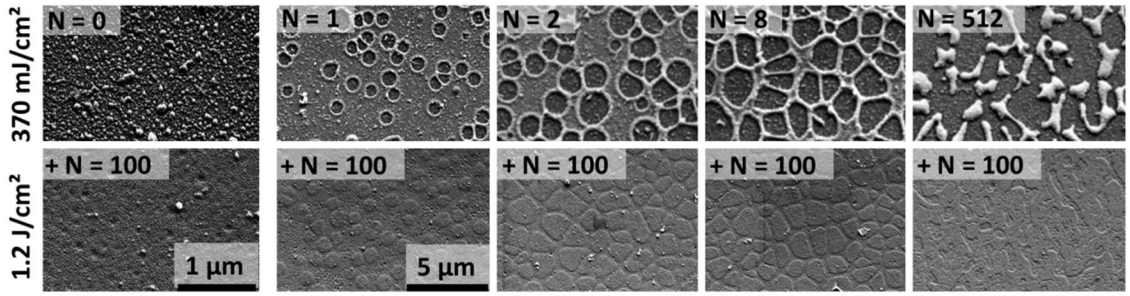

(a)

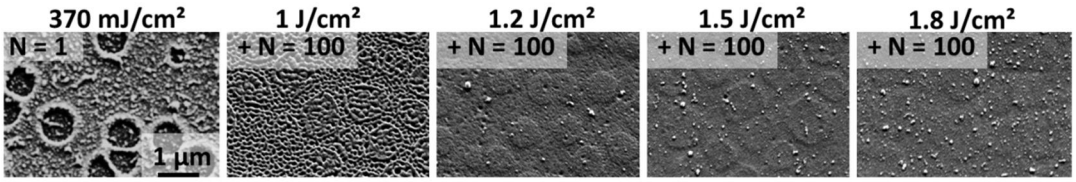

(b)

Figure 3. (a) SEM images of irradiated Mo / Al_2O_3 system,
(top) STEP 1 pre-structuring of the molybdenum layer with 370 mJ/cm² and different number of laser from 1 to 512 (in comparison to the non-treated surface N = 0)
(bottom) STEP 2 high fluence irradiated Mo/ Al_2O_3 system (Φ ≈ 1.2 J/cm², N = 100) of the pre-structures surfaces
(b) SEM images of the high fluence irradiated pre-structured Mo/ SiO_2 system (Φ = 1 – 1.8 J/cm², N = 100) where the STEP 1 (prestructuring) was performed with Φ ≈ 370 mJ/cm² and N = 1 (left image).

The high fluence irradiation of the pre-structured metal layer result in a removal of the molybdenum and to a structuring of the dielectric surface where the resultant structures are dependent on the laser fluence as well as on the geometry on the pre-structured metal layer (see Fig. 3). The geometry of the pre-structured metal layer can be adjusted by the variation of the number of laser pulses at a fixed laser fluence of ~ 370 mJ/cm² (see Fig. 3 a (top)) where the modification of the Mo layer start with a hole formation process and the increasing of the holes result in the formation of metal bar structures and finally to the formation of metal droplets. The high fluence irradiation of the different metal structures with 1.2 J/cm² and N = 100 result in a transfer of the lateral geometry of the metal structure into the sapphire surface. The resultant surface structures were measured by SEM (see Fig. 3 a (bottom)).
Furthermore, the structuring of the sapphire surface (STEP 2) is dependent on the laser fluences (see Fig. 3 b). At lower laser fluences ~ 1 J/cm² the multi-pulse irradiation result in a formation of a rough nanostructured surface where the pattern transfer is only very weak visible. At moderate laser fluences ~ 1.2 - ~ 1.5 J/cm² a very good pattern transfer was found. At higher fluences ≥ 1.8 J/cm² only a very weak or no transfer of the lateral metal geometry into the sapphire surface can be detected.

(b) nanodrilling and surface nanostructuring

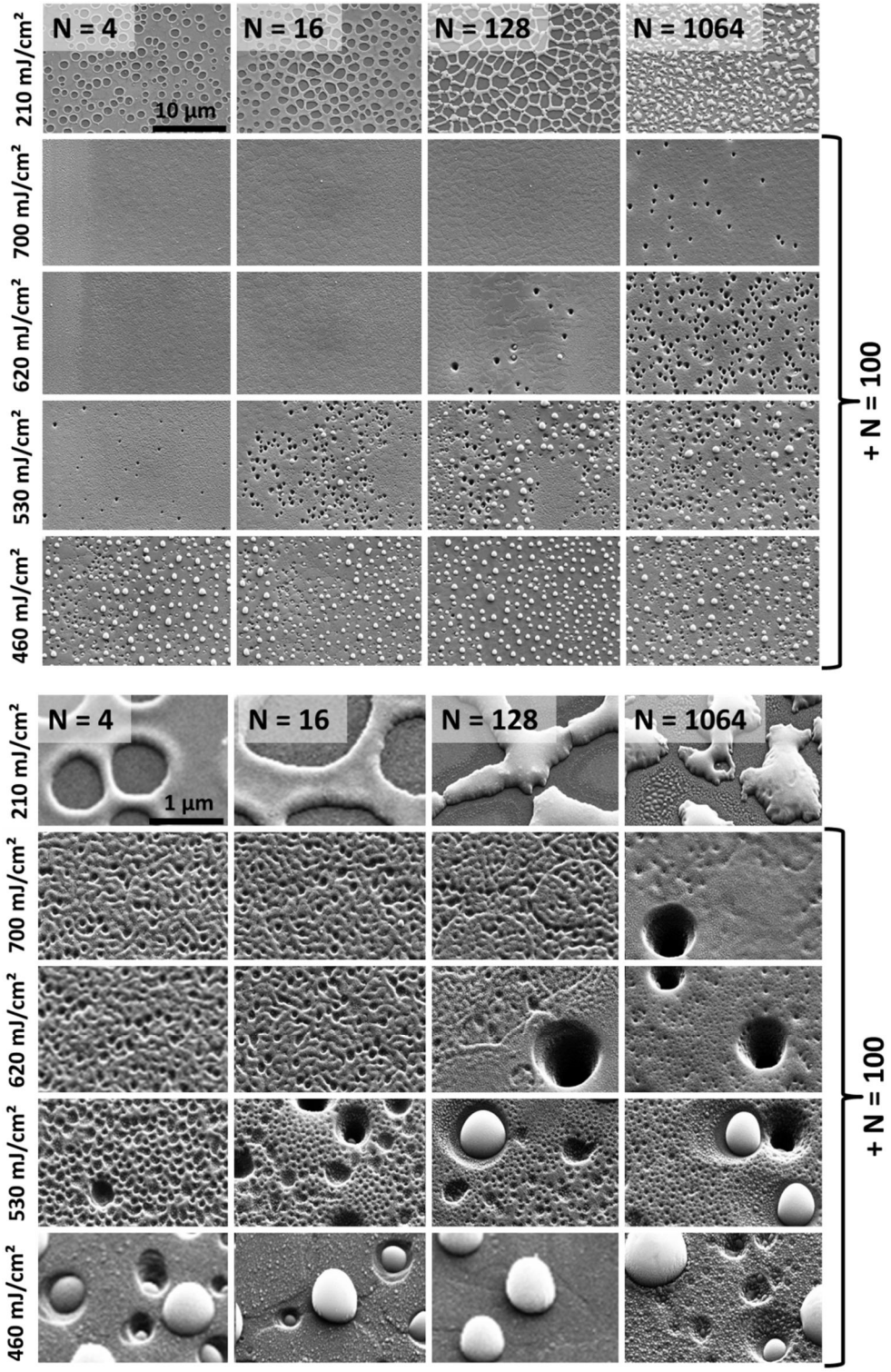

Figure 4. (a) SEM images of prestructured Mo/Al_2O_3 system with $\Phi \approx 210$ mJ/cm² and different number of laser pulses N = 1 – 1024 (top line) and high fluence irradiated prestructured Mo/Al_2O_3 system with different laser fluences $\Phi \approx 460 – 700$ mJ/cm² and N = 100 (b) SEM images of prestructured Mo/Al_2O_3 system (higher magnification) with $\Phi \approx 210$ mJ/cm² and different number of laser pulses N = 1 – 1024 (top line) and high fluence irradiated prestructured Mo/Al_2O_3 system with different laser fluences $\Phi \approx 460 – 700$ mJ/cm² and N = 100

The multi-pulse high fluence irradiation of the pre-structured Mo layer on sapphire with fluences in the range from ~ 400 to ~700 mJ/cm² result in different surface features (see Fig. 4). The irradiation result in the formation of metal droplet, the nanostructuring of the surface and a formation of deep hole structures where the different features are dependent on the laser fluence as well as on the prestructuring of the metal layer.

At lower fluences Φ ~ 460 mJ/cm² the metal droplet is the dominated feature. At higher fluences from ~ 500 to 700 mJ/cm² the irradiation result in the formation of deep hole structures where the deep hole density is dependent on the prestructuring process as well as on the laser fluence used (see Figure 5 (a)). Generally, the hole density decreased at increasing laser fluence as well as the hole density increased at increasing number of laser pulses at the prestructuring process.

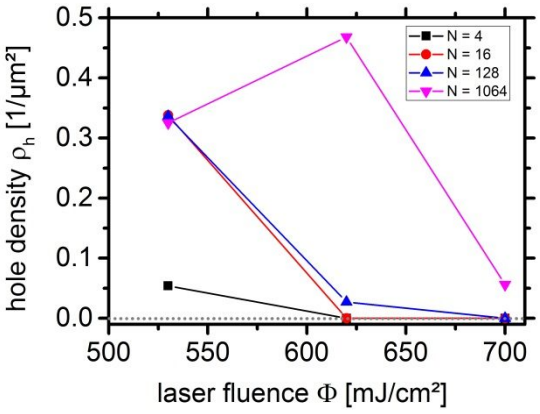

(a)

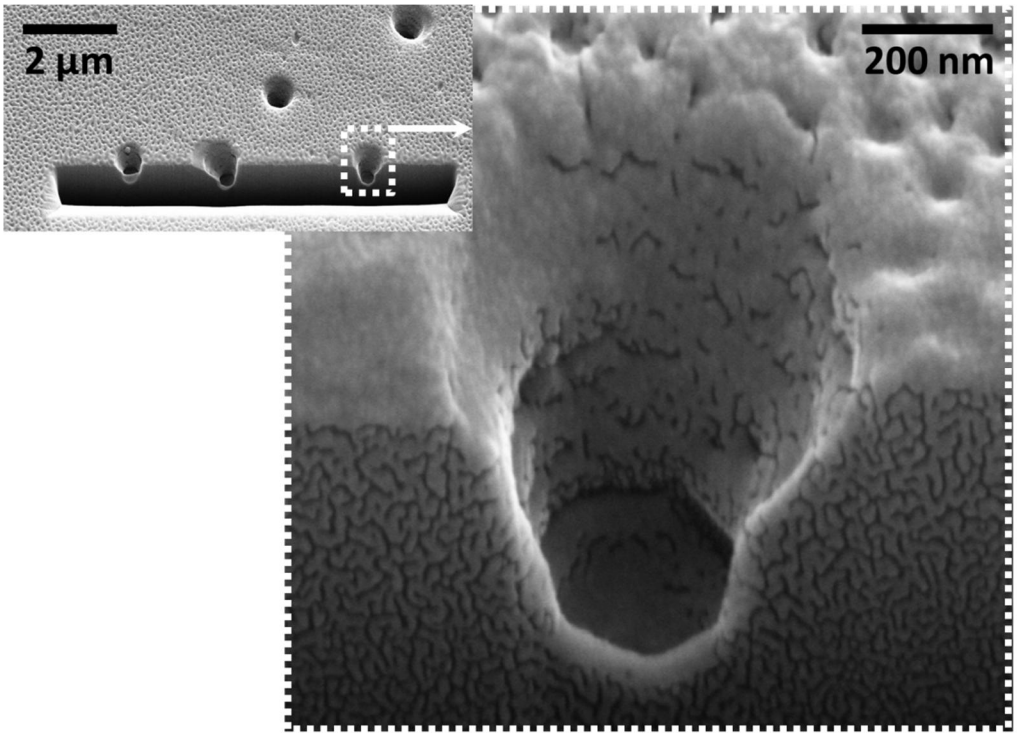

(b)

Figure 5 (a) Hole density ρ_h dependent on the laser fluence Φ at different pre-structured metal layer (Φ ~ 210 mJ/cm², N = 4 - 1024)

(b) SEM image of focused ion beam (FIB) sliced hole structure (STEP 1 (pre-structuring): Φ_p ~330 mJ/cm², N_p = 9, STEP 2 (structuring): Φ_s ~ 740 mJ/cm², N_s = 1024)

Furthermore at a laser fluence range from ~500 to ~700 mJ/cm² and small prestructuring number of laser pulses the irradiation result in a nanostructuring of the surface.
For the analysing of the hole size the irradiated system was structured by focused ion beam (FIB). A typical hole structure is shown in fig. 5 (b). At a pre-structuring parameter of Φ_p ~330 mJ/cm², $N_p = 9$ and a structuring parameter of Φ_s ~ 740 mJ/cm², $N_s = 1024$ a hole depth of ~ 450 nm and a hole diameter of ~ 600 nm can be achieved. To excluded charging effects and protection of the holes the sample was covered by 50 nm Cr at the FIB process. Further the sample was additional covered by 10 nm gold before the SEM image.

(c) application – QR code

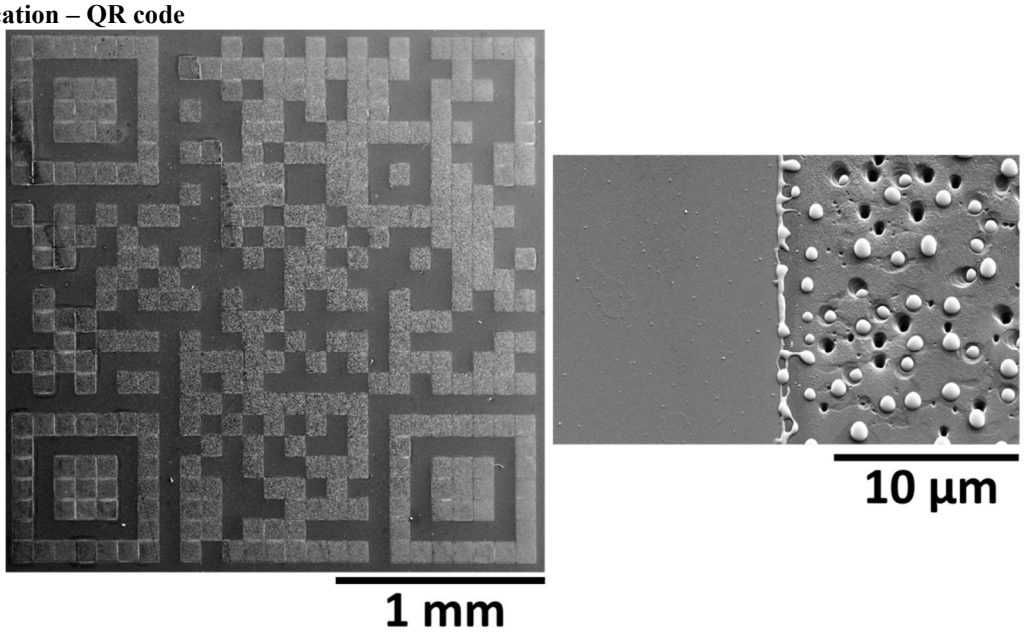

Figure 6 (left) SEM image of laser written QR code (STEP 1: Φ ~ 210 mJ/cm², N = 200; STEP 2: Φ ~500 mJ/cm², N = 200) and (right) High resolution SEM image of interface region between the irradiated and non-irradiated area.

The presented structuring method allows the localized modification of the surface of a dielectric surface like the production of metal droplets on the dielectric surface and of nanoholes in the dielectric surface. In Figure 6, the possibility of the laser structuring method is demonstrated by a QR code where the contrast is induced by the formation of metal droplet and nanoholes.

4. CONCLUSION AND OUTLOOK

i. Step 1 (low fluence irradiation)

The irradiation of the thin molybdenum layer on sapphire with low laser fluence results in a distinct modification of the surface topography where the resultant structures are dependent on the laser parameters (laser fluence Φ and number of laser pulses N). In Fig. 2a the SEM images of a laser-treated sample surface with one laser pulse and 1024 laser pulses at various laser fluences from Φ ~ 370 mJ/cm² to ~ 590 mJ/cm² are summarized. The low fluence irradiation of the molybdenum result in an melting of the metal and the surface tension of the metal liquid on the sapphire substrate result in a transformation of the molybdenum layer. At very low laser fluences Φ ≥ 370 mJ/cm² (N = 1) the transformation of the Mo layer start with the formation of hemispheric hole structures into the metal layer. The increasing of the fluence (at single pulses) result in an increase of the size of the resultant holes and finally the coalescence of the molybdenum result in the formation of metal bar and metal droplet structures (see e.g. Fig. 2 (a) N = 1, Φ = 520 mJ/cm²). A further increasing result in a formation of a metal droplet structure (see. e.g. Fig. 2 (a) Φ = 590 mJ/cm²). Similar effects can be found by multi-pulse irradiation with low laser fluences (see Fig. 2 (b)) where the resultant structure exhibit a more complex structure with structure sizes down to a few nm. This effect is most likely induced by a recrystallization of the molybdenum[42-44]. Furthermore at higher laser fluences Φ ≥ 590 mJ/cm² a structuring of the sapphire surface besides the droplet formation can be detected.

The theoretical laser fluence threshold for the melting of the molybdenum can be estimated by:

$$\Phi_{th}^{m,Mo} = \frac{\rho \cdot \Delta z}{R_{opt}} \cdot \left(c \cdot \left(T_m - 293.15\,K\right) + \Delta H_m\right) \quad (1)$$

Based on Eq. 1 and taking into account the assumed material parameters (see Tab. 1) a melting threshold of about 20 mJ/cm² can be calculated where the real threshold is higher than the theoretical value. However, for the formation of the structures is the life time of the liquid phase $\Delta\tau_{LF}$ beside the material parameter (viscosity, surface tension) important. It is knowm fror Cr on fused silica $\Delta\tau_{LF}$ increased with increasing Φ[22,45]. Based on the experiments of Cr on SiO_2[22,45] a liquid phase life time in the order of a few of tens nm up to a few µs were found. It is assumed that the values for $\Delta\tau_{LF}$ of Mo on Al_2O_3 is localized in the same order of magnitude.
Further, the attended time for complete metal dewetting process and the droplet formation process can be estimated by[37]:

$$t_d = \frac{96 \cdot \pi^3 \cdot \gamma \cdot \mu}{A_H{}^2} \cdot \Delta z^5, \quad (2)$$

respectively. Under assumption of a Hamaker parameter of $A_H \sim 10^{-18}$ J, viscosity $\mu \sim 0.004$ kg/m*s surface tension $\gamma \sim 2$ N/m [46], a t_d of a few tens of ms can be estimated.
That means, for low laser fluences the life time of the liquid phase is smaller than the attended time for the droplet formation process. Hence different structures can be produced due to the uncomplete dewetting process and the "frozen" metal structures, respectively.
The dewetting process and the resultant structures can be described very well by a modified Navier Stokes equation[23]. However, at higher number of laser pulses and higher laser fluences secondary effects like partial evaporation and crystallisation influence to resultant structures and distinct differences between the theoretical predictions and the experimental results is expected.
Besides the time-behaviour also the resultant droplet size can be estimated[37]:

$$r_D = \left[\frac{24 \cdot \pi^2 \cdot \gamma}{A_H}\right]^{1/3} \cdot \Delta z^{5/3} \quad (3)$$

Under assumption of the above mentioned paramerters a droplet radius of ~ 1 µm can be estimated. However the experimental droplet radius is obvious smaller and dependent on the laser parameter (see e.g. Fig. 2 and 4). This can be explain by a partial evaporation of the molybdenum.

ii. Step 2 (high fluence irradiation)

(a) pattern transfer

The high fluence irradiation of the prestructured metal layer on Al_2O_3 allows a transfer of the lateral geometry of the prestructred Mo into the sapphire where the resultant structures are dependent on geometry of the prestructured metal film (see Fig. 3 a) as well as on the the laser fluence (see Fig. 3 b). The best transfer can be achieved at ~ 1.2 J/cm².
At the high fluence irradiation, the laser beam is absorbed by the molybdenum structure and the localized energy transfer into the sapphire result in a localized removal of the sapphire. Two different energy transfer processes are conceivable: (i) heat transfer from laser heated Mo to Al_2O_3 and (ii) interaction of the laser produced plasma with the sapphire surface.
(i) The Mo absorbed the laser energy and result in the a increasing of the temperature of the Mo. Further, the heat conduction result in an increasing of the temperature in the sapphire nearby the Mo/Al_2O_3 interface. Finally, the complete evaporation of the Mo and partial evaporation of the Al_2O_3 result in a structuring of the sapphire substrate. This process can be physical described by a modified heat equation[37]. The model predicted, for Cr droplets on SiO_2, that the irradiation of µm and sub-µm metal structures allows µm and sub-µm the structuring of the underlying dielectric substrate, respectively, where the resultant structures is defined by the metal structures as well as by the laser fluence. The depth as well as the lateral size of the resultant structure increased with increasing laser fluence.
The theoretical prediction can explain the experimental result. A minimum energy (threshold) is necessary for the complete removal of the Mo and a partial evaporation of the Al_2O_3. The further increasing of the laser fluences induced an increasing of the lateral size of the transfer structure with less defined edges. That means, the best lateral transfer laser fluence is a little bit higher than the threshold.

(ii) At high laser fluences the irradiation of the Mo result in a fast (plasma formation time < pulse duration) formation of a plasma where the laser beam energy is partial absorbed by the formed plasma. The plasma interacted with the sapphire substrate and induced a localized removal of Al_2O_3 on the sapphire surface.
The irradiation of a homogeneous thin metal film on a dielectric surface from the front side (metal side) and from the back side presented distinct differences in the depth of the resultant structure. The back side irradiation induced deeper structures which cannot explain by a thermodynamic calculation[29]. The influence of confinement condition on the resultant structures is an indication for an energy transfer process based on a plasma –solid interaction.
Which energy transfer process dominated the structuring process is up to now unclear. However, further experiments will allow answering the question like using of a defined confinement (e.g. water film) to influence the plasma expanding.

(b) nanodrilling and surface nanostructuring
At laser energy below the threshold for the single pulse removal of the molybdenum further interesting effects can be found: a nano - roughening as well as nanodrilling of the sapphire surface (see Fig. 3).
Booth effect can be most likely explain by the multi-pulse interaction of the laser beam with the sapphire surface covered by residual Mo.
At the nanodrilling, the irradiations of formed Mo droplets result in the formation of deep holes. Similar effects were also found of Mo on fused silica[47]. The irradiation of the prestructured metal film result in the formation of the metal droplets. The further irradiation of the droplet / dielectric system results in a partial removal of the metal material and to a partial evaporation of Al_2O_3 nearby the Mo droplet. That's means, the multi-pulse irradiation induced a "burning through" of the metal droplets into the sapphire surface and forms a hole structure into the Al_2O_3 surface (see Fig. 1). The hole structuring process is restricted by the metal material, the process is finished at the complete removal of the metal inside the hole. A further analysing of the holes by SEM of focused ion beam structured samples is necessary to improve the understanding of the process.
Furthermore, the SEM presented (see Fig. 3) that the resultant hole density is dependent on the structuring fluence as well as on the prestructring process (see Fig. 4). At a constant prestructuring laser fluence, the resultant hole density increased with increasing number of prestructuring laser pulses. At Mo on SiO_2, its know that a anchoring of the metal droplet in the substrate (partial sinking of droplet into the dielectric surface) surface plays on important role at the hole formation process[47]. At Mo / Al_2O_3 also an anchoring process induced at the prestructuring process most likely influence the structuring process. Further measurements like transmission electron microscopy (TEM) are necessary to clarify this aspect.
Beside the nanoholes formation also a surface roughning at special laser parameter (see Fig. 3) can be detected. The process can be most likely explain by a surface modification of the sapphire surface at the dewetting and prestructuring process , respectively. The modification result in a reduction of the modification threshold of the non-covered dielectric surface. The high fluence irradiation result in an removal of the molybdenum and due to the modification induced reduction of the modification threshold to a nanostructuring of the sapphire surface.
For the confirmation of this thesis further measurements are necessary: analysing of the chemical surface composition by X-Ray photoelectron microscopy (XPS), analysing of the surface morphology by AFM, analysing of defects and defused metal atoms inside the Al_2O_3 by TEM.

(c) application
The presented method allows the fast and large-area localized (lateral resolution is defined by the optical resolution of the laser system used.) and self-organized surface structuring of dielectric surfaces using nanosecond laser radiation. As simple example a QR code was produced. The sample presented that the method allows the localized fabrication of nanoholes and metal droplets. The structures can be used for different application. The nanohole process can be used e.g. for the fabrication of nanosieves. The localized roughening can be used e.g. in nanofluidic system.

5. ACKNOWLEDGEMENT

We appreciate the support by the Deutsche Forschungsmeinschaft (DFG) under LO 1986/2-1.

REFERENCES

[1] B. Tan, and K. Venkatakrishnan, "A femtosecond laser-induced periodical surface structure on crystalline silicon," Journal of Micromechanics and Microengineering, 16(5), 1080-1085 (2006).
[2] M. Schade, O. Varlamova, J. Reif et al., "High-resolution investigations of ripple structures formed by femtosecond laser irradiation of silicon," Analytical and Bioanalytical Chemistry, 396(5), 1905-1911 (2010).
[3] Y. Yang, J. Yang, L. Xue et al., "Surface patterning on periodicity of femtosecond laser-induced ripples," Applied Physics Letters, 97(14), (2010).
[4] R. Le Harzic, H. Schuck, D. Sauer et al., "Sub-100 nm nanostructuring of silicon by ultrashort laser pulses," Optics Express, 13(17), 6651-6656 (2005).
[5] A. Y. Vorobyev, and C. L. Guo, "Femtosecond laser nanostructuring of metals," Optics Express, 14(6), 2164-2169 (2006).
[6] I. N. Zavestovskaya, "Laser nanostructuring of materials surfaces," Quantum Electronics, 40(11), 942-954 (2010).
[7] A. Pereira, A. Cros, P. Delaporte et al., "Surface nanostructuring of metals by laser irradiation: effects of pulse duration, wavelength and gas atmosphere," Applied Physics a-Materials Science & Processing, 79(4-6), 1433-1437 (2004).
[8] S. Imamova, A. Dikovska, N. Nedyalkov et al., "Laser nanostructuring of thin Au films for application in surface enhanced Raman spectroscopy," Journal of Optoelectronics and Advanced Materials, 12(3), 500-504 (2010).
[9] S. J. Henley, C. H. P. Poa, A. Adikaari et al., "Excimer laser nanostructuring of nickel thin films for the catalytic growth of carbon nanotubes," Applied Physics Letters, 84(20), 4035-4037 (2004).
[10] K. Ratautas, M. Gedvilas, G. Raciukaitis et al., "Nanoparticle formation after nanosecond-laser irradiation of thin gold films," Journal of Applied Physics, 112(1), (2012).
[11] V. N. Tokarev, "Mechanism of laser drilling superhigh-aspect-ratio holes in polymers," Quantum Electronics, 36(7), 624-637 (2006).
[12] M. Mendes, J. Park, "Wafer processing with short-pulsed UV DPSS lasers expanding new applications development," Advanced Packaging 15 (3), 37-40 (2006).
[13] K. Sugioka, J. Xu, D. Wu et al., "Femtosecond laser 3D micromachining: a powerful tool for the fabrication of microfluidic, optofluidic, and electrofluidic devices based on glass," Lab on a Chip, 14(18), 3447-3458 (2014).
[14] Y. Qi, H. Qi, A. Chen et al., "Improvement of aluminum drilling efficiency and precision by shaped femtosecond laser," Applied Surface Science, 317, 252-256 (2014).
[15] Y. V. White, X. Li, Z. Sikorski et al., "Single-pulse ultrafast-laser machining of high aspect nano-holes at the surface of SiO2," Optics Express, 16(19), 14411-14420 (2008).
[16] Q. Zhang, H. Lin, B. Jia et al., "Nanogratings and nanoholes fabricated by direct femtosecond laser writing in chalcogenide glasses," Optics Express, 18(7), 6885-6890 (2010).
[17] R. Boehme, K. Zimmer, D. Ruthe et al., "Backside Etching at the Interface to Diluted Medium with Nanometer Etch Rates," Journal of Laser Micro Nanoengineering, 1(3), 190-194 (2006).
[18] K. Zimmer, R. Boehme, C. Vass et al., "Time-resolved measurements during backside dry etching of fused silica," Applied Surface Science, 255(24), 9617-9621 (2009).
[19] M. Ehrhardt, G. Raciukaitis, P. Gecys et al., "Microstructuring of fused silica by laser-induced backside wet etching using picosecond laser pulses," Applied Surface Science, 256(23), 7222-7227 (2010).
[20] P. Lorenz, M. Ehrhardt, and K. Zimmer, "Laser-induced front side etching of fused silica with KrF excimer laser using thin chromium layers," Physica Status Solidi a-Applications and Materials Science, 209(6), 1114-1118 (2012).
[21] P. Lorenz, F. Frost, M. Ehrhardt et al., "Laser-induced fabrication of randomly distributed nanostructures in fused silica surfaces," Applied Physics a-Materials Science & Processing, 111(4), 1025-1030 (2013).
[22] P. Lorenz, M. Kloeppel, T. Smausz et al., "Time dependency of the laser-induced nanostructuring process of chromium layers with different thicknesses on fused silica," Applied Surface Science, 336, 176-181 (2015).
[23] P. Lorenz, M. Kloeppel, F. Frost et al., "Laser-induced circular nanostructures in fused silica assisted by a self-assembling chromium layer," Applied Surface Science, 280, 933-939 (2013).
[24] E. Matthias, M. Reichling, J. Siegel et al., "THE INFLUENCE OF THERMAL-DIFFUSION ON LASER-ABLATION OF METAL-FILMS," Applied Physics a-Materials Science & Processing, 58(2), 129-136 (1994).
[25] S. J. Henley, J. D. Carey, and S. R. P. Silva, "Pulsed-laser-induced nanoscale island formation in thin metal-on-oxide films," Physical Review B, 72(19), (2005).
[26] D. Bäuerle, [Laser Processing and Chemistry] Springer, Heidelberg(2011).

[27] R. F. Wood, and G. E. Giles, “MACROSCOPIC THEORY OF PULSED-LASER ANNEALING .1. THERMAL TRANSPORT AND MELTING,” Physical Review B, 23(6), 2923-2942 (1981).
[28] P. Lorenz, M. Ehrhardt, A. Wehrmann et al., “Laser-induced front side etching of fused silica with XeF excimer laser using thin metal layers,” Applied Surface Science, 258(23), 9138-9142 (2012).
[29] P. Lorenz, M. Ehrhardt, and K. Zimmer, “Laser-induced front side and back side etching of fused silica with KrF and XeF excimer lasers using metallic absorber layers: A comparison,” Applied Surface Science, 258(24), 9742-9746 (2012).
[30] P. Lorenz, M. Ehrhardt, K. Zimmer, “Laser-induced front side etching of fused silica with short and ultra-short laser pulses", Proc. SPIE 8243, Laser Applications in Microelectronic and Optoelectronic Manufacturing (LAMOM) XVII, 82430Y (February 9, 2012); doi:10.1117/12.907929; http://dx.doi.org/10.1117/12.907929
[31] A. Sharma, and R. Khanna, “Pattern formation in unstable thin liquid films,” Physical Review Letters, 81(16), 3463-3466 (1998).
[32] A. Yochelis, E. Knobloch, and L. M. Pismen, “Formation and mobility of droplets on composite layered substrates,” European Physical Journal E, 22(1), 41-49 (2007).
[33] A. Vrij, “POSSIBLE MECHANISM FOR SPONTANEOUS RUPTURE OF THIN FREE LIQUID FILMS,” Discussions of the Faraday Society(42), 23-& (1966).
[34] C. Favazza, R. Kalyanaraman, and R. Sureshkumar, “Robust nanopatterning by laser-induced dewetting of metal nanofilms,” Nanotechnology, 17(16), 4229-4234 (2006).
[35] D. A. Willis, and X. Xu, “Transport phenomena and droplet formation during pulsed laser interaction with thin films,” Journal of Heat Transfer-Transactions of the Asme, 122(4), 763-770 (2000).
[36] J. Trice, D. Thomas, C. Favazza et al., “Pulsed-laser-induced dewetting in nanoscopic metal films: Theory and experiments,” Physical Review B, 75(23), (2007).
[37] P. Lorenz, M Klöppel, F. Frost, M. Ehrhardt, P. Li and K. Zimmer, “Nanostructuring of fused silica surfaces induced by KrF excimer laser radiation: Experiment and theory,” NSTI - Nanotech 1 (2013) 686 - 689, ISBN 978-1-4822-0581-7
[38] Gruneisen, Handbuch der Physik, vol. 10, Springer, Berlin, 1926
[39] S. Elhadj, M. J. Matthews, S. T. Yang et al., “Evaporation kinetics of laser heated silica in reactive and inert gases based on near-equilibrium dynamics,” Optics Express, 20(2), 1575-1587 (2012).
[40] S. Preuss, A. Demchuk, and M. Stuke, “SUBPICOSECOND UV LASER-ABLATION OF METALS,” Applied Physics a-Materials Science & Processing, 61(1), 33-37 (1995).
[41] D. A. Ditmars, S. Ishihara, S. S. Chang et al., “ENTHALPY AND HEAT-CAPACITY STANDARD REFERENCE MATERIAL - SYNTHETIC SAPPHIRE (ALPHA-AL2O3) FROM 10 TO 2250 K,” Journal of Research of the National Bureau of Standards, 87(2), 159-163 (1982).
[42] Y. Zhang, L. Liu, G. Zou et al., “Femtosecond laser-induced phase transformations in amorphous Cu77Ni6Sn10P7 alloy,” Journal of Applied Physics, 117(2), (2015).
[43] K. Brendel, N. H. Nickel, P. Lengsfeld et al., “Excimer laser crystallization of amorphous silicon on metal coated glass substrates,” Thin Solid Films, 427(1-2), 86-90 (2003).
[44] K. Sakaike, S. Higashi, H. Murakami et al., “Crystallization of amorphous Ge films induced by semiconductor diode laser annealing,” Thin Solid Films, 516(11), 3595-3600 (2008).
[45] P.-F. Paradis, T. Ishikawa, N. Koike, “Non-contact measurements of the surface tension and viscosity of molybdenum using an electrostatic levitation furnace,” International Journal of Refractory Metals & Hard Materials 25, 95–100 (2007).
[46] P. F. Paradis, T. Ishikawa, and N. Koike, “Non-contact measurements of the surface tension and viscosity of molybdenum using an electrostatic levitation furnace,” International Journal of Refractory Metals & Hard Materials, 25(1), 95-100 (2007).
[47] P. Lorenz, J. Zajadacz, L. Bayer et al., “Nanodrilling of fused silica using nanosecond laser radiation,” Applied Surface Science, 351, 935-945 (2015).